

# Spatial Downscaling of SMAP Soil Moisture Using MODIS Land Surface Temperature and NDVI During SMAPVEX15

Andreas Colliander<sup>1</sup>, Senior Member, IEEE, Joshua B. Fisher, Gregory Halverson, Olivier Merlin, Sidharth Misra<sup>2</sup>, Senior Member, IEEE, Rajat Bindlish<sup>2</sup>, Senior Member, IEEE, Thomas J. Jackson, Fellow, IEEE, and Simon Yueh, Fellow, IEEE

**Abstract**—The Soil Moisture Active Passive (SMAP) mission provides a global surface soil moisture (SM) product at 36-km resolution from its L-band radiometer. While the coarse resolution is satisfactory to many applications, there are also a lot of applications which would benefit from a higher resolution SM product. The SMAP radiometer-based SM product was downscaled to 1 km using Moderate Resolution Imaging Spectroradiometer (MODIS) data and validated against airborne data from the Passive Active L-band System instrument. The downscaling approach uses MODIS land surface temperature and normalized difference vegetation index to construct soil evaporative efficiency, which is used to downscale the SMAP SM. The algorithm was applied to one SMAP pixel during the SMAP Validation Experiment 2015 (SMAPVEX15) in a semiarid study area for validation of the approach. SMAPVEX15 offers a unique data set for testing SM downscaling algorithms. The results indicated reasonable skill (root-mean-square difference of 0.053 m<sup>3</sup>/m<sup>3</sup> for 1-km resolution and 0.037 m<sup>3</sup>/m<sup>3</sup> for 3-km resolution) in resolving high-resolution SM features within the coarse-scale pixel. The success benefits from the fact that the surface temperature in this region is controlled by soil evaporation, the topographical variation within the chosen pixel area is relatively moderate, and the vegetation density is relatively low over most parts of the pixel. The analysis showed that the combination of the SMAP and MODIS data under these conditions can result in a high-resolution SM product with an accuracy suitable for many applications.

**Index Terms**—Land surface temperature (LST), Moderate Resolution Imaging Spectroradiometer (MODIS), normalized difference vegetation index (NDVI), Passive Active L-band System (PALS), soil moisture (SM), Soil Moisture Active Passive (SMAP).

Manuscript received July 2, 2017; revised August 19, 2017; accepted September 11, 2017. Date of publication October 6, 2017; date of current version October 25, 2017. This work was supported in part by the Jet Propulsion Laboratory Advanced Earth Missions Program, in part by the National Aeronautics and Space Administration (NASA) SMAP Project, and in part by the NASA SUSMAP Program under Grant NNN13D503T. (Corresponding author: Andreas Colliander.)

A. Colliander, J. B. Fisher, G. Halverson, S. Misra, and S. Yueh are with the Jet Propulsion Laboratory, California Institute of Technology, Pasadena, CA 91109 USA (e-mail: andreas.colliander@jpl.nasa.gov).

O. Merlin is with the Centre d'Etudes Spatiales de la Biosphère, Ecohydrologie, 31401 Toulouse, France (e-mail: olivier.merlin@cesbio.cnes.fr).

R. Bindlish is with the NASA Goddard Space Flight Center, Greenbelt, MD 20771 USA (e-mail: rajat.bindlish@nasa.gov).

T. J. Jackson is with the USDA Agricultural Research Service, Hydrology and Remote Sensing Laboratory, Beltsville, MD 20705 USA (e-mail: tom.jackson@ars.usda.gov).

Color versions of one or more of the figures in this letter are available online at <http://ieeexplore.ieee.org>.

Digital Object Identifier 10.1109/LGRS.2017.2753203

## I. INTRODUCTION

SOIL moisture (SM) has a critical role in water and energy balance processes at the interface between the land surface and atmosphere. It determines the partitioning of the incoming solar and atmospheric radiation into latent, sensible, and ground heat fluxes, and the partitioning of the precipitation into surface runoff and infiltration. It has an important impact on agricultural and irrigation management practices, food production, and the organization of natural ecosystems and biodiversity. Low-frequency passive microwave remote sensing has been established as the primary tool for global retrieval of SM due to its sensitivity to subsurface SM and relative insensitivity to vegetation [1]. The NASA Soil Moisture Active Passive (SMAP) [3] and European Space Agency Soil Moisture Ocean Salinity (SMOS) [2] missions utilize L-band radiometers to map global SM every 2–3 days. Both missions use instrument technologies that result in aperture sizes that provide data with a spatial resolution of about 40 km [4], [5]. However, many applications would benefit from significantly finer spatial resolution (see [6]). SMAP also originally included an L-band synthetic aperture radar at 1–3-km resolution, which was intended to downscale the radiometer-based SM measurements to a 9-km resolution [7]. However, the radar failed after about three months of operation. In this letter, an alternative downscaling approach is applied to SMAP data.

Several approaches have been proposed for SM downscaling. Some of them use fine-resolution microwave measurements (see [8], [9]), and some use measurements at optical wavelengths (see [10]–[13]). These algorithms include approaches where thermal infrared land surface temperature (LST) signatures are used as the main source of information to disaggregate the coarse-resolution SM pixels into finer ones. The algorithm applied in this letter to downscale the coarse-resolution SMAP radiometer-based SM product is based on the relationship between soil evaporative efficiency (SEE) and SM [14]. In [15], an operational algorithm for SMOS downscaling with Moderate Resolution Imaging Spectroradiometer (MODIS) data using the SEE–SM relationship was presented.

In order to assess the quality of the downscaled SM values, reference SM observations are required. *In situ* measurement

networks are typically used in SM validation. However, they are not optimal for assessing the spatial patterns that the downscaling approaches are set to resolve. Problems arise from resolution cell representation, station-to-station biases, and consistency of data records. A more robust approach is to use a higher resolution remote-sensing instrument to capture the spatial patterns. Airborne microwave radiometers at L-band frequency can achieve much finer resolution than that of their spaceborne counterparts. A field experiment for SM validation of SMAP was conducted in Southern Arizona in August 2015 called SMAP Validation Experiment 2015 (SMAPVEX15). In this experiment, an airborne L-band instrument Passive Active L-band Sensor (PALS) was deployed to measure an area consisting of three SMAP pixels on seven days. The SMAPVEX15 data set offers a uniquely appropriate reference SM data set for testing the algorithm for two reasons. First, the SM disaggregation methods utilizing LST perform optimally when the surface temperature is mainly controlled by soil evaporation. This is generally the case in the SMAPVEX15 domain. Second, testing a downscaling algorithm requires some spatial heterogeneity in the measured SM fields. The experiment was designed to coincide with the North American monsoon, which resulted in small-scale convective precipitation events that created very heterogeneous scenes in terms of SM [16].

Here, we present the results of SMAP SM product downscaling using MODIS data over the SMAPVEX15 domain and validation with the PALS 1-km SM measurements.

## II. DISAGGREGATION ALGORITHM

The higher resolution SM is estimated using the difference between the high-resolution SEE and average SEE within the coarser-scale pixel. This difference is multiplied by the relationship of SM and SEE before adding to the SM retrieved with SMAP

$$SM = SM_{SMAP} + \frac{\partial SM}{\partial SEE}(SEE - \langle SEE \rangle_C) \quad (1)$$

where  $SM_{SMAP}$  is the SMAP SM for the pixel (coarse resolution) [ $m^3/m^3$ ];  $\partial SM/\partial SEE$  is the partial derivative of SM evaluated with respect to SEE [ $m^3/m^3$ ]; SEE denotes SEE at the 1-km resolution [-]; and  $\langle SEE \rangle_C$  is the spatially averaged SEE [-], in which  $C$  stands for coarse scale. SEE is estimated as follows:

$$SEE = \frac{T_{s,max} - T_s}{T_{s,max} - T_{s,min}} \quad (2)$$

where the soil skin temperature [K] is defined as

$$T_s = \frac{T_{MODIS} - f_v(T_{v,min} + T_{v,max})/2}{1 - f_v} \quad (3)$$

and the end members of soil (subscript  $s$ ) and vegetation (subscript  $v$ ) temperature  $T_{s,min}$ ,  $T_{s,max}$ ,  $T_{v,min}$ , and  $T_{v,max}$  are estimated as described in the following.  $T_{MODIS}$  stands for the altitude-corrected LST from MODIS [K], and  $f_v$  is the fractional vegetation cover [-] estimated as follows:

$$f_v = \frac{NDVI_{MODIS} - NDVI_s}{NDVI_b - NDVI_s} \quad (4)$$

where  $NDVI_{MODIS}$  is the normalized difference vegetation index from MODIS [-], and  $NDVI_s$  and  $NDVI_b$  stand for NDVI fraction for bare and full vegetation cover, respectively. The altitude effect on the surface temperature is accounted for within each pixel using a coefficient of 6 °C/km as given in [17].

The end members of the temperature range are determined within the coarse-scale pixel following the approach presented in [17], accounting for the fact that the selected pixel in the SMAPVEX15 domain has a generally low amount of vegetation with  $f_v < 0.5$

$$\begin{aligned} T_{s,min} &= \min(T_{MODIS}) \\ T_{v,min} &= \min(T_{MODIS}) \\ T_{s,max} &= \max(T_{MODIS}) \\ T_{v,max} &= \max\left(\frac{T_{MODIS} - T_{s,max}(1 - f_v)}{f_v}\right). \end{aligned} \quad (5)$$

A critical part in the algorithm is the estimation of  $\partial SM/\partial SEE$ . In this letter, the following approximation was used:

$$\partial SM/\partial SEE = a \frac{1}{N} \sum_{i=1}^N \frac{SM_{SMAP,i}}{\langle SEE \rangle_{C,i}} \quad (6)$$

where  $N$  is the number of days and  $a$  is an experimental tuning parameter;  $a = 0.5$  was used in the subsequent analysis. The partial derivative could have been resolved from linear regression between SEE and SM if the time series had been longer, but with the available time period, these results turned out to be unreliable. This led to simpler approach used here. The tuning parameter  $a$  was introduced to enable the investigation of the sensitivity of the SEE-based downscaling approach to SM variation without the influence of the additional error sources.

## III. DATA

### A. SMAPVEX15 and PALS Soil Moisture Data

The SMAPVEX15 field experiment was carried out in Southern Arizona, USA, (31.7°N, 110.3°W) between August 2 and 18, 2015 [16]. The objective of the experiment was the validation of SMAP SM products, particularly to obtain a data set for assessment of spatial downscaling techniques. The campaign domain extended over three 36-km SMAP pixels that were covered with the airborne PALS instrument seven times. *In situ* SM measurements consisted of a permanent network that was augmented with a temporary network and manual sampling. The location and timing of the experiment were chosen to capture spatially heterogeneous SM conditions. In this region, the North American monsoon generates small-scale convective storms that can result in highly variable SM [18]. The landscape of the region is characterized by shrub and grass rangeland. The domain includes significant variation in elevation with lowest points at about 1000 m above mean sea level (MSL) and mountains reaching 2600 m above MSL. This has a notable impact on the LST distribution, and subsequent SM, across the domain. Fig. 1 shows the digital elevation model (DEM) and NDVI on August 2, 2015 based on MODIS. The analysis in this letter focuses on the SMAP

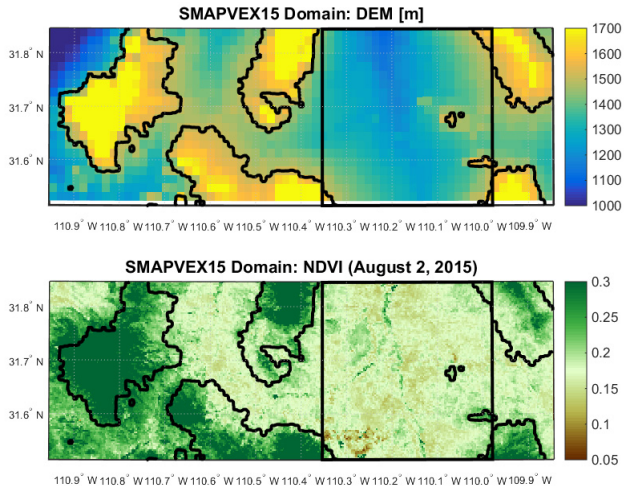


Fig. 1. SMAPVEX15 experimental domain. (a) DEM. (b) NDVI on August 2, 2015. The square denotes the 5-km pixel used in the analysis and contours show the areas with elevation higher than 1500 m.

pixel outlined in the figure with a square. Within this particular pixel area, the elevation variation and amount of vegetation are moderate. See [16] for more details about the experimental domain.

The PALS instrument collects coincident (in time and place) radar and radiometer measurements [19]. Both measurements are obtained through the same antenna in a fast-switching sequence. PALS has been used in several SM studies in the past in various configurations (see [20]–[24]). During SMAPVEX15, PALS was installed on a dc-3 aircraft. For SMAPVEX15, the flights were made at an altitude of 2300 m above ground. The instrument provides a footprint of 1100 m (along scan) by 1500 m (radially) on the ground with an effective resolution of about 1200 m (square root of the area of the footprint ellipse). The PALS brightness temperature observations were translated into SM as described in [16]. The SM was assessed with respect to *in situ* measurements in the Walnut Gulch Experimental Watershed (WGEW); the RMSD was found to be  $0.016 \text{ m}^3/\text{m}^3$  and the correlation 0.83.

### B. SMAP Soil Moisture Data

The SMAP Level 2 SM Passive (L2SMP) product was used. Details of the SMAP L2SMP algorithm are presented in [25]. The baseline algorithm uses vertically polarized brightness temperature and a single-channel algorithm [26]. The SM retrieval takes place on the SMAP 36-km EASE-2 grid. Because the grid samples the ground in intervals of 36 km, SMAP developed an additional process for retrieving the 36-km SM at 3-km intervals. This so-called validation grid processing allows placing the 36-km retrieval pixels optimally with respect to *in situ* stations to reduce uncertainties arising from misalignment of the retrieval and the ground-based reference data. A centered validation grid pixel was defined over the WGEW. The analysis here focuses on the 6 A.M. overpasses, which is the nominal observation time for SMAP, because it is expected that early morning surface and vegetative thermal conditions are more consistent with the isothermal assumptions made in the retrieval algorithm.

### C. MODIS Data

The daily L3 MODIS/Terra LST and emissivity product on the global 1-km grid (MOD11A1, Version 5) was used for LST [27], and the 16-day L3 MODIS/Terra vegetation index product on the global 500-m grid (MOD13A1, Version 5) was used for NDVI [28]. The local overpass time for the data acquisitions was around 10:30 A.M. The LST data were resampled, and NDVI data aggregated onto a 1-km grid over the domain. The quality flags of MOD11A1 were used to screen out LST data of questionable quality for determining the soil and vegetation end members (see Section II). Only MODIS data with a quality flag that showed good quality were used with one exception. It was allowed that the average emissivity error was within 0.02 (as opposed to 0.01) because this significantly increased the available data. The quality flagging procedure resulted in the omission of the second (August 5) and the last PALS flight day (August 18).

## IV. RESULTS

The algorithm described in Section II was applied to the SMAP and MODIS data on each PALS flight day over the pixel highlighted in Fig. 1. The area was required to be at least 50% cloud free, which was the case on the PALS flight days. As mentioned earlier, the SMAP pixel was chosen so that the downscaled area does not include large elevation changes, which would cause artifacts even with the elevation compensation (due to illumination effects [29]). The pixel contains only light to moderate vegetation, except for the narrow riparian areas. Denser vegetation is found at higher altitudes in this region. The low vegetation density simplified the retrieval because it made the partitioning between vegetation and soil temperature less critical.

Fig. 2 shows the downscaled SMAP SM with PALS SM. The maps indicate that most of the SM patterns observed with PALS are successfully replicated with the downscaling process. In some cases, the magnitude of SM is notably different while the patterns are still clearly identifiable (such as on August 2). Some artifacts can be identified as well. For example, on August 13 in the southeastern corner, the wet areas do not correspond to PALS SM. This may be the result of poor quality LST data because some of the quality flags are raised around this area. The NDVI map in Fig. 1 shows the riparian area in the middle of the pixel. The downscaled SM on August 13 and 16 appear to have a systematic difference in the SM between the east and west sides of the river, but this does not correspond to the PALS SM. Different sides of the river (with opposite elevation gradients) may experience different temperature dynamics, which is the likely cause for this effect.

Fig. 3 shows the scatterplots and metrics for the comparison of the downscaled SMAP SM and the PALS SM. Fig. 3(a) shows the result for 1-km resolution, and Fig. 3(b) shows the results after averaging both the downscaled and PALS SM to 3-km resolution. In both cases, the mean difference is very small (but nonzero). The unbiased root-mean-square difference (ubRMSD) decreases, and the Pearson correlation ( $R$ ) increases with averaging, which is expected. The performance

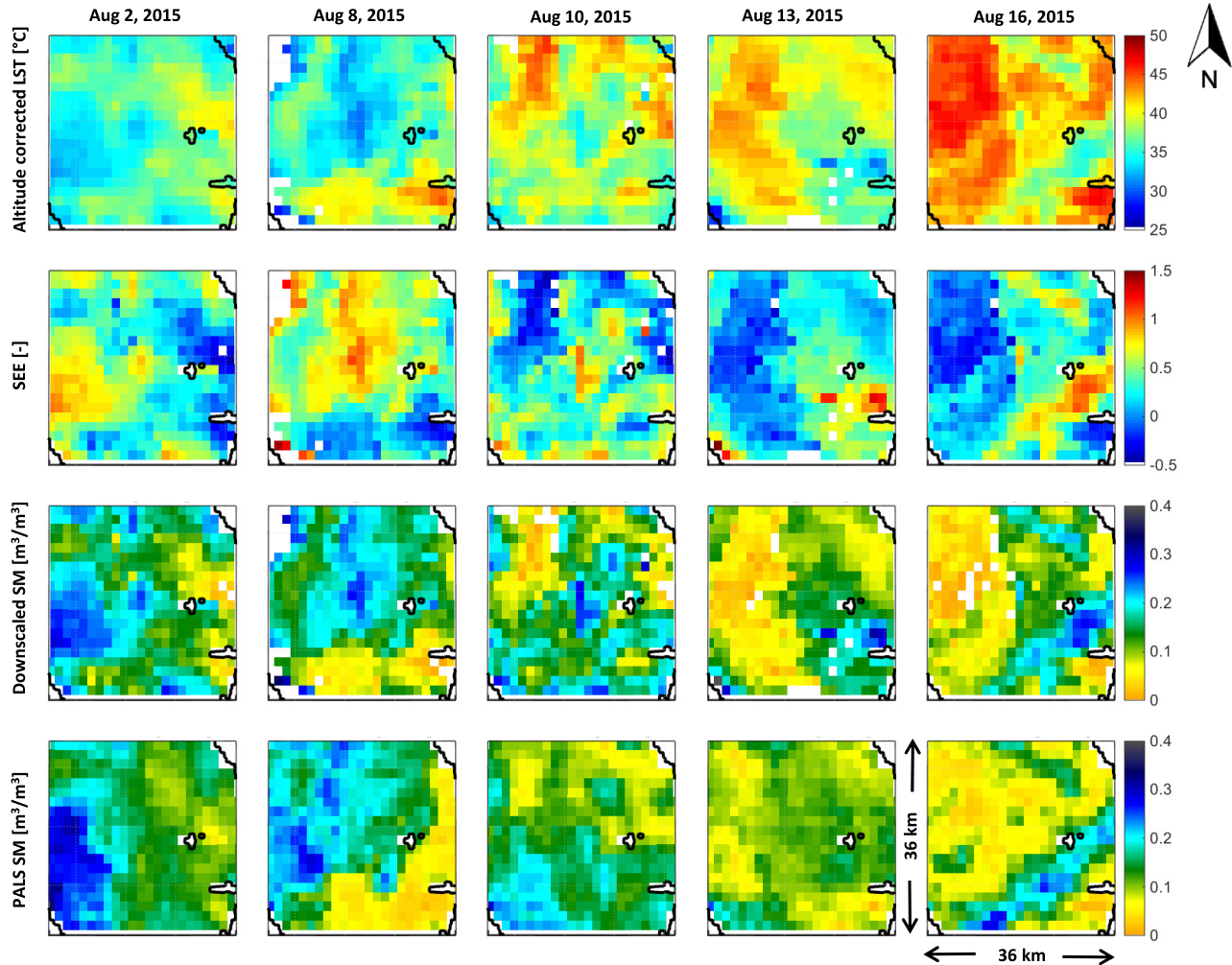


Fig. 2. SMAP pixel area on the five PALS flight days. (First row) Altitude-corrected MODIS LST. (Second row) SEE. (Third row) Downscaled SMAP SM. (Fourth row) PALS SM.

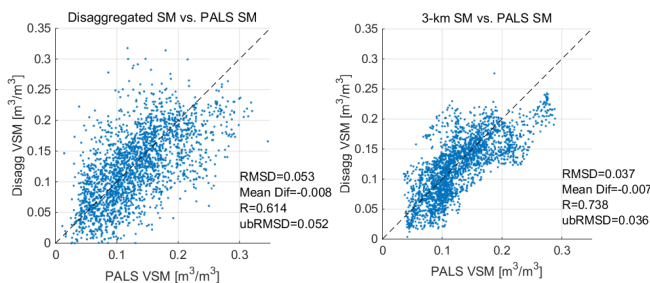


Fig. 3. Downscaled SMAP SM with respect to the PALS SM. (Left) 1-km resolution. (Right) 3-km resolution. The dots represent all 1-km and 3-km pixels within the coarse-scale grid cell on the five PALS flight days.

is comparable to that reported in the literature for similar types of retrieval situations (see [15], [30], [31]). Notably, the performance at the 3-km resolution meets the SMAP performance requirement of  $0.04 \text{ m}^3/\text{m}^3$  ubRMSD [32].

The uncertainty of the original SMAP SM contributes to the uncertainty of the downscaled SM. In order to quantify the effect of that uncertainty in this comparison, the aggregated PALS SM within the pixel area was also downscaled using the same algorithm. The results were close to those reported in Fig. 3 (for 1 km, both RMSD and ubRMSD  $0.052 \text{ m}^3/\text{m}^3$ , mean difference  $0 \text{ m}^3/\text{m}^3$ , and correlation  $0.655$ ; for 3 km,

both RMSD and ubRMSD  $0.035 \text{ m}^3/\text{m}^3$ , mean difference  $0 \text{ m}^3/\text{m}^3$ , and correlation  $0.783$ ). When compared to Fig. 3, the main difference is the zero-mean difference. The ubRMSD and correlation are also slightly better, but it can be concluded that differences between PALS and SMAP SMs are not the drivers in the error figures. This was also expected based on the fact that [16] showed that the aggregated PALS SM was very close to SMAP SM.

The main source of error in the algorithm is the SM–SEE relationship. In addition, factors that could potentially degrade the comparison results include differences in observation depth and in observation time between the satellites. LST is very sensitive to temperature at the surface of the soil or vegetation, whereas L-band microwaves penetrate several centimeters into the ground depending on the wetness conditions. As such, when SMAP and PALS made their measurements early in the morning, and MODIS at 10:30 A.M., not only the sensing depth was different but also conditions may have changed, especially in the top surface.

## V. CONCLUSION

A downscaling analysis of the SMAP coarse-resolution radiometer-based SM product using MODIS data was con-

ducted for a semiarid rangeland site. The approach uses LST- and NDVI-based SEE to downscale the SMAP SM. The algorithm was applied over one pixel in the SMAPVEX15 domain, and the downscaled SM was compared with airborne-based high-resolution SM. The combination of the small-scale variability of SM, soil evaporation controlling the surface temperature, and availability of the airborne high-resolution SM measurement offered a unique opportunity to test this algorithm. The results showed that the algorithm, adopted from the previous work presented in the literature, demonstrated reasonable skill in resolving higher resolution SM features within the coarse-scale pixel. The analysis of the approach benefited from the features of the study domain: the surface temperature is controlled by soil evaporation, the topographical variation within the pixel area is relatively moderate, and the vegetation density is relatively low over most parts of the pixel. (The latter two aspects also contribute to the reliability of the SMAP SM product.) The analysis presented shows that the combination of the SMAP and MODIS data under these conditions can result in a high-resolution SM product with an accuracy suitable for many applications.

#### ACKNOWLEDGMENT

This research was carried out at the Jet Propulsion Laboratory, California Institute of Technology, Pasadena, CA, USA. The data used are listed in the references and available through NASA LP (<http://lpdaac.usgs.gov/>) and NSIDC DAAC (<http://nsidc.org>).

#### REFERENCES

- [1] T. Schmugge, P. E. O'Neill, and J. R. Wang, "Passive microwave soil moisture research," *IEEE Trans. Geosci. Remote Sens.*, vol. GE-24, no. 1, pp. 12–22, Jan. 1986.
- [2] S. Mecklenburg *et al.*, "ESA's Soil Moisture and Ocean Salinity mission: From science to operational applications," *Remote Sens. Environ.*, vol. 180, pp. 3–18, Jul. 2016.
- [3] D. Entekhabi *et al.*, "The Soil Moisture Active Passive (SMAP) mission," *Proc. IEEE*, vol. 98, no. 5, pp. 704–716, May 2010.
- [4] J. R. Piepmeier *et al.*, "SMAP L-band microwave radiometer: Instrument design and first year on orbit," *IEEE Trans. Geosci. Remote Sens.*, vol. 55, no. 4, pp. 1954–1966, Apr. 2017.
- [5] K. D. McMullan *et al.*, "SMOS: The payload," *IEEE Trans. Geosci. Remote Sens.*, vol. 46, no. 3, pp. 594–605, Mar. 2008.
- [6] J. Peng, A. Loew, O. Merlin, and N. E. C. Verhoest, "A review of spatial downscaling of satellite remotely sensed soil moisture," *Rev. Geophys.*, vol. 55, no. 2, pp. 341–366, 2017.
- [7] N. N. Das, D. Entekhabi, E. G. Njoku, J. J. C. Shi, J. T. Johnson, and A. Colliander, "Tests of the SMAP combined radar and radiometer algorithm using airborne field campaign observations and simulated data," *IEEE Trans. Geosci. Remote Sens.*, vol. 52, no. 4, pp. 2018–2028, Apr. 2014.
- [8] U. Narayan, V. Lakshmi, and T. J. Jackson, "High-resolution change estimation of soil moisture using L-band radiometer and Radar observations made during the SMEX02 experiments," *IEEE Trans. Geosci. Remote Sens.*, vol. 44, no. 6, pp. 1545–1554, Jun. 2006.
- [9] X. Wu, J. P. Walker, C. Rüdiger, R. Panciera, and Y. Gao, "Intercomparison of alternate soil moisture downscaling algorithms using active-passive microwave observations," *IEEE Geosci. Remote Sens. Lett.*, vol. 14, no. 2, pp. 179–183, Feb. 2017.
- [10] N. S. Chauhan, S. Miller, and P. Ardanuy, "Spaceborne soil moisture estimation at high resolution: A microwave-optical/IR synergistic approach," *Int. J. Remote Sens.*, vol. 24, no. 22, pp. 4599–4622, 2003.
- [11] M. Piles *et al.*, "Downscaling SMOS-derived soil moisture using MODIS visible/infrared data," *IEEE Trans. Geosci. Remote Sens.*, vol. 49, no. 9, pp. 3156–3166, Sep. 2011.
- [12] B. Fang, V. Lakshmi, R. Bindlish, T. J. Jackson, M. Cosh, and J. Basara, "Passive microwave soil moisture downscaling using vegetation index and skin surface temperature," *Vadose Zone J.*, 2013, doi: [10.2136/vzj2013.05.0089](https://doi.org/10.2136/vzj2013.05.0089).
- [13] J. Peng, A. Loew, S. Zhang, J. Wang, and J. Niesel, "Spatial downscaling of satellite soil moisture data using a vegetation temperature condition index," *IEEE Trans. Geosci. Remote Sens.*, vol. 54, no. 1, pp. 558–566, Jan. 2016.
- [14] O. Merlin, J. P. Walker, A. Chehbouni, and Y. Kerr, "Towards deterministic downscaling of SMOS soil moisture using MODIS derived soil evaporative efficiency," *Remote Sens. Environ.*, vol. 112, no. 10, pp. 3935–3946, 2008.
- [15] B. Molero *et al.*, "SMOS disaggregated soil moisture product at 1 km resolution: Processor overview and first validation results," *Remote Sens. Environ.*, vol. 180, pp. 361–376, Jul. 2016.
- [16] A. Colliander *et al.*, "Validation and scaling of soil moisture in a semi-arid environment: SMAP validation experiment 2015 (SMAPVEX15)," *Remote Sens. Environ.*, vol. 196, pp. 101–112, Jul. 2017.
- [17] O. Merlin, M. J. Escorihuela, M. A. Mayoral, O. Hagolle, A. A. Bitar, and Y. Kerr, "Self-calibrated evaporation-based disaggregation of SMOS soil moisture: An evaluation study at 3 km and 100 m resolution in Catalunya, Spain," *Remote Sens. Environ.*, vol. 130, pp. 25–38, Mar. 2013.
- [18] D. K. Adams and A. C. Comrie, "The North American monsoon," *Bull. Amer. Meteorol. Soc.*, vol. 78, no. 10, pp. 2197–2213, 1997.
- [19] W. J. Wilson *et al.*, "Passive active L- and S-band (PALS) microwave sensor for ocean salinity and soil moisture measurements," *IEEE Trans. Geosci. Remote Sens.*, vol. 39, no. 5, pp. 1039–1048, May 2001.
- [20] E. G. Njoku *et al.*, "Observations of soil moisture using a passive and active low-frequency microwave airborne sensor during SGP99," *IEEE Trans. Geosci. Remote Sens.*, vol. 40, no. 12, pp. 2659–2673, Dec. 2002.
- [21] R. Bindlish, T. Jackson, R. Sun, M. Cosh, S. Yueh, and S. Dinardo, "Combined passive and active microwave observations of soil moisture during CLASIC," *IEEE Geosci. Remote Sens. Lett.*, vol. 6, no. 4, pp. 644–648, Oct. 2009.
- [22] A. Colliander *et al.*, "Long term analysis of PALS soil moisture campaign measurements for global soil moisture algorithm development," *Remote Sens. Environ.*, vol. 121, pp. 309–322, Jun. 2012.
- [23] A. Colliander *et al.*, "Retrieving soil moisture for non-forested areas using PALS radiometer measurements in SMAPVEX12 field campaign," *Remote Sens. Environ.*, vol. 184, pp. 86–100, Oct. 2016.
- [24] M. Barber, C. Bruscatini, F. Grings, and H. Karszenbaum, "Bayesian combined active/passive (B-CAP) soil moisture retrieval algorithm," *IEEE J. Sel. Topics Appl. Earth Observ. Remote Sens.*, vol. 9, no. 12, pp. 5449–5460, Dec. 2016.
- [25] S. Chan *et al.*, "Assessment of the SMAP passive soil moisture product," *IEEE Trans. Geosci. Remote Sens.*, vol. 54, no. 8, pp. 4994–5007, Aug. 2016.
- [26] T. J. Jackson, "Measuring surface soil moisture using passive microwave remote sensing," *Hydrol. Process.*, vol. 7, no. 2, pp. 139–152, 1993.
- [27] Z. Wan. (1999). "MODIS land-surface temperature algorithm theoretical basis document (LST ATBD)," Inst. Comput. Earth Syst. Sci., Univ. California, Santa Barbara, Santa Barbara, CA, USA, MODIS LST ATBD Version 3.3. [Online]. Available: [http://modis.gsfc.nasa.gov/data/atbd/atbd\\_mod11.pdf](http://modis.gsfc.nasa.gov/data/atbd/atbd_mod11.pdf)
- [28] A. Huete, C. Justice, and W. van Leeuwen. (1999). "MODIS vegetation index (MOD 13) algorithm theoretical basis document," Dept. Environ. Sci., NASA, Washington, DC, USA, MOD13 ATBD Version 3. [Online]. Available: [http://modis.gsfc.nasa.gov/data/atbd/atbd\\_mod13.pdf](http://modis.gsfc.nasa.gov/data/atbd/atbd_mod13.pdf)
- [29] Y. Malbêteau *et al.*, "Normalizing land surface temperature data for elevation and illumination effects in mountainous areas: A case study using ASTER data over a steep-sided valley in Morocco," *Remote Sens. Environ.*, vol. 189, pp. 25–39, Feb. 2017.
- [30] N. Djamali, R. Magagi, K. Goita, O. Merlin, Y. Kerr, and A. Walker, "Disaggregation of SMOS soil moisture over the Canadian Prairies," *Remote Sens. Environ.*, vol. 170, pp. 255–268, Dec. 2015.
- [31] Y. Malbêteau, O. Merlin, B. Molero, C. Rüdiger, and S. Bacon, "DisPATCH as a tool to evaluate coarse-scale remotely sensed soil moisture using localized *in situ* measurements: Application to SMOS and AMSR-E data in Southeastern Australia," *Int. J. Appl. Earth Observ. Geoinf.*, vol. 45, pp. 221–234, Mar. 2016.
- [32] A. Colliander *et al.*, "Validation of SMAP surface soil moisture products with core validation sites," *Remote Sens. Environ.*, vol. 191, pp. 215–231, Mar. 2017.